Assessing sub-cellular resolution in spatial proteomics experiments

Laurent Gatto* [1,2], Lisa M. Breckels[1,2], and Kathryn S. Lilley[2]

[1] *Computational Proteomics Unit, Department of Biochemistry, University of Cambridge, Tennis Court Road, Cambridge, CB2 1QR, UK*
[2] *Cambridge Centre for Proteomics, Department of Biochemistry, University of Cambridge, Tennis Court Road, Cambridge, CB2 1QR, UK*

July 25, 2018

Abstract

The sub-cellular localisation of a protein is paramount in defining its function, and a protein's mis-localisation is known to lead to adverse effect. As a result, numerous experimental techniques and datasets have been published, with the aim to decipher localisation of proteins at various scales and resolutions, including high profile mass spectrometry-based efforts. Here, we present a tool, termed *QSep*, and a meta-analysis assessing and comparing the sub-cellular resolution of 28 such mass spectrometry-based spatial proteomics experiments.

*lg390@cam.ac.uk

1 Introduction

In biology, the localisation of a protein to its intended sub-cellular niche is a necessary condition for it to assume its biological function. Indeed, the localisation of a protein will determine its specific biochemical environment and its unique set of interaction partners. As a result, the same protein can assume different functions in different biological contexts and its mis-localisation can lead to adverse effects and has been implicated in multiple diseases [22, 5, 23].

Spatial proteomics is the systematic and high-throughput study of protein sub-cellular localisation. A wide range of techniques (reviewed in [10, 25]) and computational methods [11] have been documented, that confidently infer the localisation of thousands of proteins. Most techniques rely on some form of sub-cellular fractionation, many employing differential centrifugation or separation along density gradients, and the subsequent quantitative assessment of relative protein occupancy profiles in these sub-cellular fractions. Reciprocally, a broad array of computational methods have been applied, ranging from unsupervised learning e.g. clustering [27] and dimensionality reduction, and supervised learning e.g. classification (reviewed in [11]), semi-supervised learning and novelty detection [2] and, more recently, transfer learning [3] and Bayesian modelling [6].

Despite these advances, there is surprisingly little agreement in the community as to what constitutes a reliable spatial proteomics experiment, i.e a dataset that generates confident protein assignment results. Is is however implicit that reliability and trust in the results is dependent on adequate sub-cellular resolution, i.e. *enough* separation between the different sub-cellular niches being studied to be able to confidently discern protein profiles originating from different sub-cellular niches. And yet, every spatial proteomics publication will somehow arbitrarily claim to have obtained satisfactory resolution.

The importance of adequate sub-cellular resolution reaches beyond the generation of reliable static spatial maps. It is a necessary property of the data to consider tackling more subtle sub-cellular patterns such as multi- and trans-localisation, i.e. the localisation of proteins in multiple sub-cellular niches and the relocation of proteins upon perturbation [11].

In this work, we describe how to understand and interpret widely used dimensionality reduction methods and visualise spatial proteomics data to

critically assess their resolution. We propose a simple, yet effective method to quantitatively measure resolution and compare it across different experiments. Our recommendations should be useful to spatial proteomics practitioners, to assess the sub-cellular resolution of their experiments and compare it to similar studies while setting up and optimising their experiments, as well biologists interested in critically assessing spatial proteomics studies and their claims.

All the data and software used in this work is available in the `pRoloc` and `pRolocdata` packages [12]. The code to reproduce all results and figures presented here are available in the source of the document, available in the manuscript public repository [9].

2 Spatial proteomics datasets

For this meta-analysis, we make use of 29 spatial proteomics datasets, summarised in table 1. These data represent a diverse range of species, sample types, instruments and quantification methodologies.

Data	Proteins	Fractions	Clusters	PC var (%)	Title
hyperLOPIT2015	5032	20	14	72.26	Protein and PMS-level hyperLOPIT datasets on Mouse E14TG2a embryonic stem cells from Christoforou et al. (2016). [4]
hyperLOPIT2015ms2	7114	10	14	74.72	Protein and PMS-level hyperLOPIT datasets on Mouse E14TG2a embryonic stem cells from Christoforou et al. (2016). [4]
HEK293T2011	1371	8	12	65.04	LOPIT experiment on Human Embryonic Kidney fibroblast HEK293T cells from Breckels et al. (2013) [2]
hirst2018	2046	15	12	82.50	Data from Hirst et al. 2018 [15]
hyperLOPITU2OS2017	5020	40	12	63.29	2017 hyperLOPIT on U2OS cells [26] (all fractions)
hyperLOPITU2OS2017b	5020	37	12	67.68	2017 hyperLOPIT on U2OS cells [26] (cleaned)
itzhak2016stcSILAC	5265	30	12	70.61	Data from Itzhak et al. (2016) [16]
itzhak2017	9201	30	12	31.39	Data from Itzhak et al. 2017 [17]
rodriguez2012r1	2215	11	12	38.95	Spatial proteomics of human inducible goblet-like LS174T cells from Rodriguez-Pineiro et al. (2012) [21]
tan2009r1	888	4	11	88.49	LOPIT data from Tan et al. (2009) [24]
E14TG2aS1	1109	8	10	65.98	LOPIT experiment on Mouse E14TG2a Embryonic Stem Cells from Breckels et al. (2016) [3]
trotter2010	347	16	10	81.14	LOPIT data sets used in Trotter et al. (2010) [28]
beltran2016HCMV120	2045	6	9	79.36	Data from Beltran et al. 2016 [18] HCMV infection, 120 hpi (hours post-infection)
beltran2016HCMV24	2196	6	9	77.18	Data from Beltran et al. 2016 [18] HCMV infection, 24 hpi
beltran2016HCMV48	2206	6	9	74.95	Data from Beltran et al. 2016 [18] HCMV infection, 48 hpi
beltran2016HCMV72	2062	6	9	75.32	Data from Beltran et al. 2016 [18] HCMV infection, 72 hpi

beltran2016HCMV96	1868	6	9	76.59	Data from Beltran et al. 2016 [18] HCMV infection, 96 hpi
beltran2016MOCK120	1757	6	9	71.84	Data from Beltran et al. 2016 [18] MOCK, 120 hpi
beltran2016MOCK24	2220	6	9	80.12	Data from Beltran et al. 2016 [18] MOCK, 24 hpi
beltran2016MOCK48	2181	6	9	68.90	Data from Beltran et al. 2016 [18] MOCK, 48 hpi
beltran2016MOCK72	2161	6	9	68.83	Data from Beltran et al. 2016 [18] MOCK, 72 hpi
beltran2016MOCK96	1748	6	9	73.24	Data from Beltran et al. 2016 [18] MOCK, 96 hpi
dunkley2006	689	16	9	86.70	LOPIT data from Dunkley et al. (2006) [7]
foster2006	1555	26	8	53.13	PCP data from Foster et al. (2006) [8]
nikolovski2014	1385	20	8	67.97	LOPIMS data from Nikolovski et al. (2014) [20]
groen2014cmb	424	18	7	64.30	LOPIT experiments on Arabidopsis thaliana roots, from Groen et al. (2014) [13]
nikolovski2012imp	1385	32	7	77.82	Meta-analysis from Nikolovski et al. (2012) [19]
andreyev2010rest	2642	36	6	25.39	Six sub-cellular fraction data from mouse macrophage-like RAW264.7 cells from Andreyev et al. (2009) [1]
hall2009	1090	16	5	63.45	LOPIT data from Hall et al. (2009) [14]

Table 1: Summary of the datasets used in this study. The percentage of variance along the principal components (PC) is related to the PCA plots on figure 12. All datasets are available in the `pRolocdata` package.

We have applied minimal post-processing to the data and have used, as far as possible, the data and annotation provided by the original authors. The data from Foster et al. [8] have been annotated using the curated marker list from Christoforou et al. [4], as only a limited number of markers were provided by the authors[1]. We have also only considered sub-cellular niches (also referred to as protein clusters, or clusters) that were defined by at least 7 protein markers[2]. We used combined dataset of multiple replicated experiments, when provided by the original authors, rather than individual replicates, as combining data often leads to better sub-cellular resolution [28]. In addition, for dimensionality reduction and visualisation, we have systematically replaced missing values by zeros. When calculating distances between protein profiles (see section 3.3), however, missing values were retained.

It is important to highlight that not all experiments used in this study have as main goal the generation of a global (or near global) sub-cellular map. While the works of Dunkley et al. [7] (*Mapping the Arabidopsis organelle proteome*), Tan et al. [24] (*Mapping organelle proteins and protein complexes in Drosophila melanogaster*) and more recently Christoforou et al. [4] (*A draft map of the mouse pluripotent stem cell spatial proteome*) and Itzhak et al. [16] (*Global, quantitative and dynamic mapping of protein subcellular localization*) explicitly state such goal, other experiments such as Groen et al. [13] (*Identification of trans-golgi network proteins in Arabidopsis thaliana root tissue*) or Nikolovski et al. [20] (*Label free protein quantification for plant Golgi protein localisation and abundance*) have a more targeted goal (identification of trans-Golgi -network and Golgi apparatus proteins, respectively). When an experiment is targeted at resolving a particular niche, it is often the case that other sub-compartments are less well-resolved and hence, it is important to keep the overall aim of the studies in mind when assessing their resolution.

[1]This results from the fact that they used a simple distance measurement, termed χ^2, against very few markers to base their sub-cellular localisation prediction

[2]This number is relatively low, and we would typically recommend at least 13 markers per class to perform cross-validation when optimising classifier parameters. See Gatto et al. [11] and the main `pRoloc` tutorial for details.

3 Assessment

3.1 Sub-cellular diversity

A first assessment that provides an important indication of the resolution of the data concerns the number and diversity of sub-cellular niches that are annotated. In the 29 datasets used in this study, this number ranged from 5 (dataset *hall2009*) to 14 (dataset *hyperLOPIT2015*). These numbers should be assessed in the light of about 25 different sub-cellular niches that are documented in all 29 datasets, which are still underestimating the biological sub-cellular diversity.

3.2 Dimensionality reduction and visualisation

Principal component analysis (PCA) is a widely used dimensionality reduction technique in spatial proteomics. It projects the protein occupancy profiles into a new space in such a way as to maximise the spread of all points (i.e. labelled and unlabelled proteins) along the first new dimension (principal component, PC). The second PC is then chosen to be perpendicular to the first one while still maximising the remaining variability. Each PC (there are as many as there are channels) accounts for a percentage of the total variability and it is not uncommon, in well executed experiments, that the two first PCs summarise over 70% of the total variance in the data, confirming that the resulting visualisation remains a reliable and useful simplification of the original multidimensional data.

By firstly summarising the occupancy profiles along PC1 and PC2 (and, possibly, other PCs of interest if necessary), it becomes possible to visualise the complete dataset in a single figure (as opposed to individual sets of profiles - see for example figure 5 in Gatto et al. [10]). In a first instance, it is advised to visualise the data without annotation to confirm the presence of discrete clusters, i.e. dense clouds of points that are well separated from the rest of the data (see for example data from Christoforou et al. [4] on figure 1, left). Such patterns can further be emphasised by using transparency (figure 1, centre) or binned hexagon plots (figure 1, right) to highlight density.

In figure 2 we compare three datasets to illustrate different levels of cluster density and separation. We see areas of high density (many proteins per hexagon) are highlighted by dark blue, and less dense areas are white/grey, as indicated by the count key on the right-hand side of each plot. The

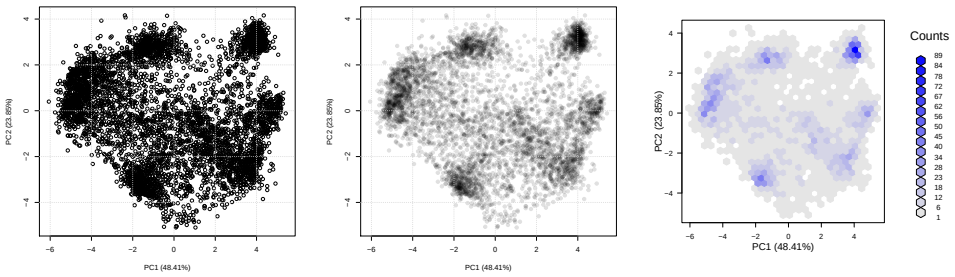

Figure 1: Unsupervised visualisation of spatial resolution using the `plot2D` function from the `pRoloc` package.

figure on the left is the hyperLOPIT data from Christoforou et al. [4] (as on figure 1) that used synchronous precursor selection (SPS) MS^3 on an Orbitrap Fusion. The middle figure represents the same experiment and same proteins, analysed using conventional MS^2, illustrating the effect of reduced quantitation accuracy. Finally, on the right, an experiment with considerable less resolution [14].

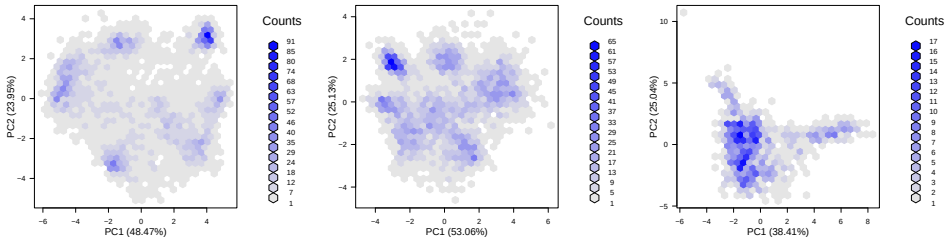

Figure 2: Comparing the cluster density and separation of experiments with excellent (left), intermediate (centre) and poor (right) resolution.

Considering that the aim of sub-cellular fractionation is to maximise separation of sub-cellular niches, one would expect sub-cellular clusters to be separated optimally in a successful spatial proteomics experiment. In PCA space, this would equate to the location of the annotated spatial clusters along the periphery of the data points. In other words, the maximum variability of a successful spatial proteomics experiments should be reflected by the separation of the expected/annotated spatial clusters, as illustrated on

figure 3.

As already mentioned in section 3.1, sub-cellular niches observed in spatial proteomics are usually annotated. This annotation comes in the form of marker proteins, i.e. well-known and trusted residents of a specific niche, for the species and condition of interest.

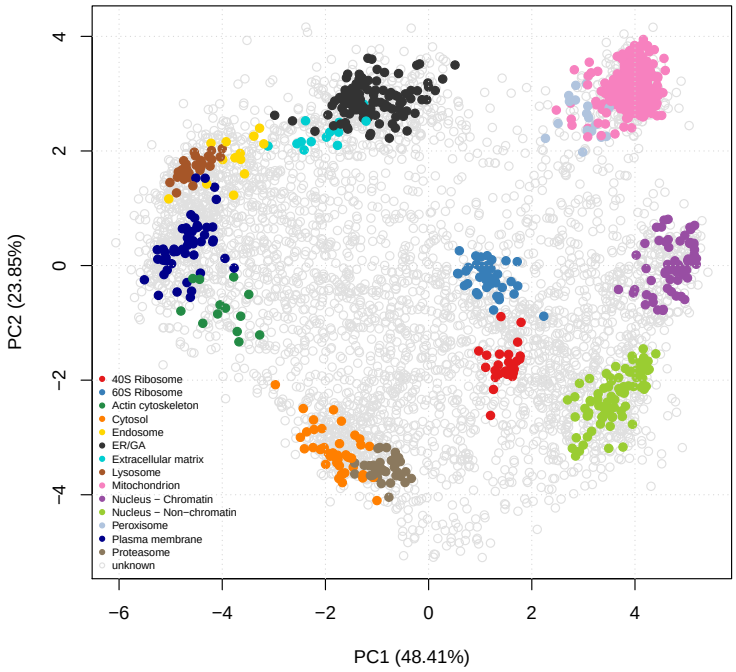

Figure 3: Annotated PCA plot of the *hyperLOPIT2015* dataset.

Another dimensionality reduction method that is worth mentioning here is linear discriminant analysis (LDA). LDA will project the protein occupancy profiles in a new set of dimensions using as a criterion the separation of marker classes by maximising the between class variance to the within class variance ratio. As opposed to the *unsupervised* PCA, the *supervised* LDA should not be used as an experiment quality control, but can be useful to assess if one or more organelles have been preferentially separated.

It is important to highlight that these representations, while reflecting a major fraction of the variability in the data, are only a summary of the to-

tal variability. Some sub-cellular niches that overlap in 2 dimensions can be separated along further components. It is sometimes useful to visualise data in three dimensions (using for example the `plot3D` function in the `pRoloc` package), which still, however, only reflect part of the total variability. When assessing the resolution of some organelles of interest, one should compare the full protein profiles of the marker proteins (`pRoloc`'s `plotDist` function can be used for this, or the interactive application `pRolocVis` in the `pRolocGUI` package) or visualise a dendrogram representing the average distance between cluster profiles (the `mrkHClust` function from `pRoloc` offers this functionality). While detailed exploration of a dataset using these and other visualisation approaches is crucial before analysing and interpreting a new spatial proteomics experiment, a detailed exploration of each of the 29 datasets used in this meta-analysis is out of the scope of this analysis.

3.3 Quantifying resolution

While visualisation of spatial proteomics data remains essential to assess the resolution, and hence the success, of a spatial proteomics experiment, it is useful to be able to objectively quantify the resolution and directly compare different experiments. Here, we present a new infrastructure, termed `QSep`, available in the `pRoloc` package Gatto et al. [12], to quantify the separation of clusters in spatial proteomics experiments. It relies on the comparison of the average euclidean distance *within* and *between* sub-cellular clusters. As illustrated on the heatmaps in figure 4 for the *hyperLOPIT2015* data, these distances always refer to one reference marker cluster.

The raw distance matrix (figure 4, top-left) is symmetrical (i.e. the distance between cluster 1 and 2 is the same as between cluster 2 and 1). Within distances are generally the smallest ones, except when two clusters overlap, as the lysosome and endosome in our example. To enable the comparison of these distances within and between experiments (see section 4 for the latter), we further divide each distance by the reference within cluster average distance (figure 4, top-right). This thus informs us as how much the average distance between cluster 1 and 2 is greater than the average distance within cluster 1 (i.e. the tightness of that cluster). At this stage, the distance matrix is no longer symmetrical. To facilitate the comparison of distances between organelles, the distance distributions can also be visualised as boxplots (figure 4, bottom).

The rational behind these measures is as follows. Intuitively, we assess

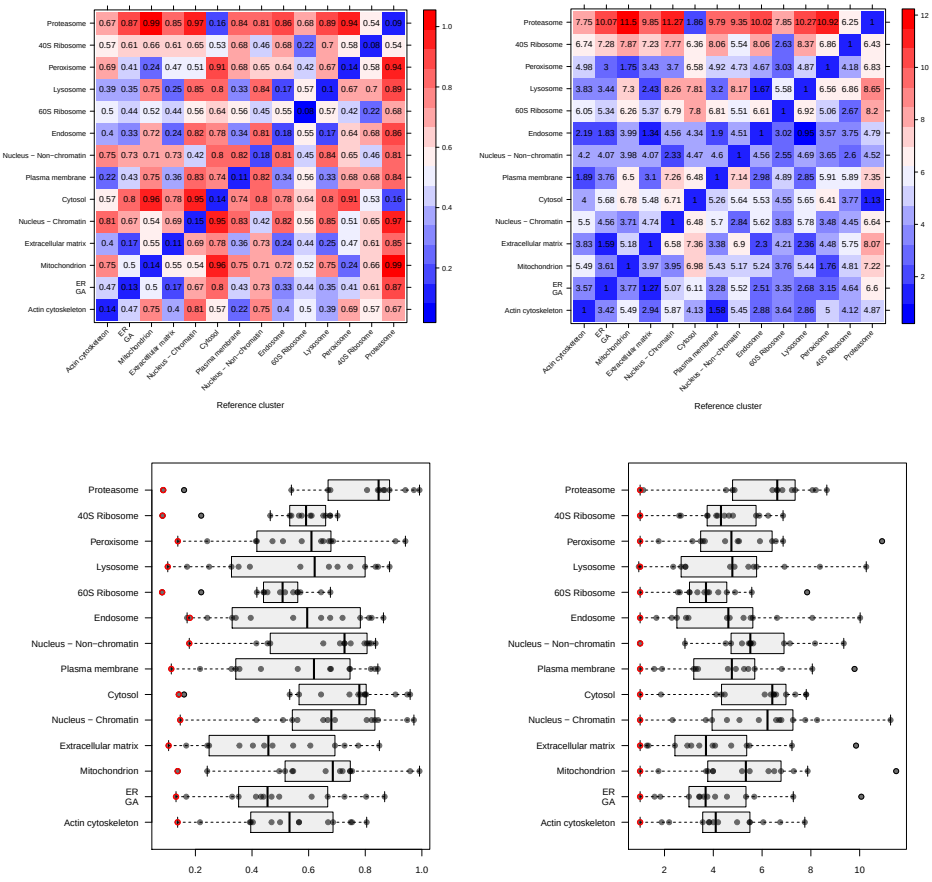

Figure 4: Quantifying resolution of the *hyperLOPIT2015* data Christoforou et al. [4]. The heatmaps at the top illustrate the raw (left) and average normalised (right) within (along the diagonal) and between euclidean cluster distances. The boxplots at the bottom summarise these same values (raw on the left, normalised on the right) to enable easier comparison between clusters, where the within distances are highlighted in red.

resolution by contrasting the separation between clusters (formalised by the average distance between two clusters) and the tightness of single clusters (formalised by the average within cluster distance). Ideal sub-cellular fractionation would yield tight and distant clusters, represented by a large normalised between cluster distances on figure 4.

3.4 Application of the assessment criteria

To further demonstrate the interpretation of these resolution metrics, we directly compare the two recent global cell maps from [4] (dataset *hyperLOPIT2015*) and [16] (dataset *itzhak2016stcSILAC*). Both feature high protein coverage (7114 and 5265 proteins respectively) and good sub-cellular diversity (14 and 12 annotated clusters respectively). The former contains duplicated experiments, each made of 10 fractions and the latter contains 6 replicates with 5 fractions each. Figure 5 shows the PCA plots applying transparency to identify the underlying structure in the quantitative data and the annotated versions using the markers provided by the respective authors.

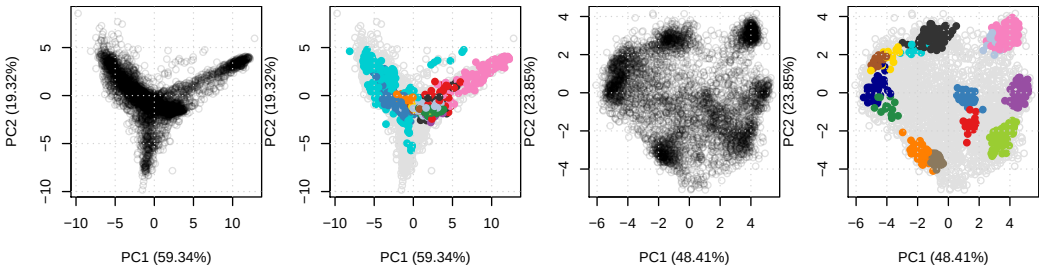

Figure 5: PCA plots for *itzhak2016stcSILAC* (left) and *hyperLOPIT2015* (right). Here, we display PC 1 and 2 for both datasets for comparability. The original authors displayed PC 1 and 3 for the *itzhak2016stcSILAC* data (see figures 11 and 12 below).

Figure 6 illustrates the normalised distance heatmaps and boxplots for the two datasets (*itzhak2016stcSILAC* at the top and *hyperLOPIT2015* at the bottom). The two heatmaps display strikingly different colour patterns. The top heatmap shows a majority of small normalised distances (blue cells) and with only a limited number of large distances (red cells), along the mitochondrial reference cluster. Conversely, the bottom heatmap displays a majority of average (white cells) and large distances (red cells) across all sub-cellular clusters. The boxplots allow a more direct comparison of the distances across the two datasets. On the top boxplot, we detect relatively short distances for most clusters, with most large distances stemming from the mitochondria, leading to a median distance of 2.48. The distributions on the bottom boxplot show larger distances, equally spread among all clusters, with an median distance of 4.91.

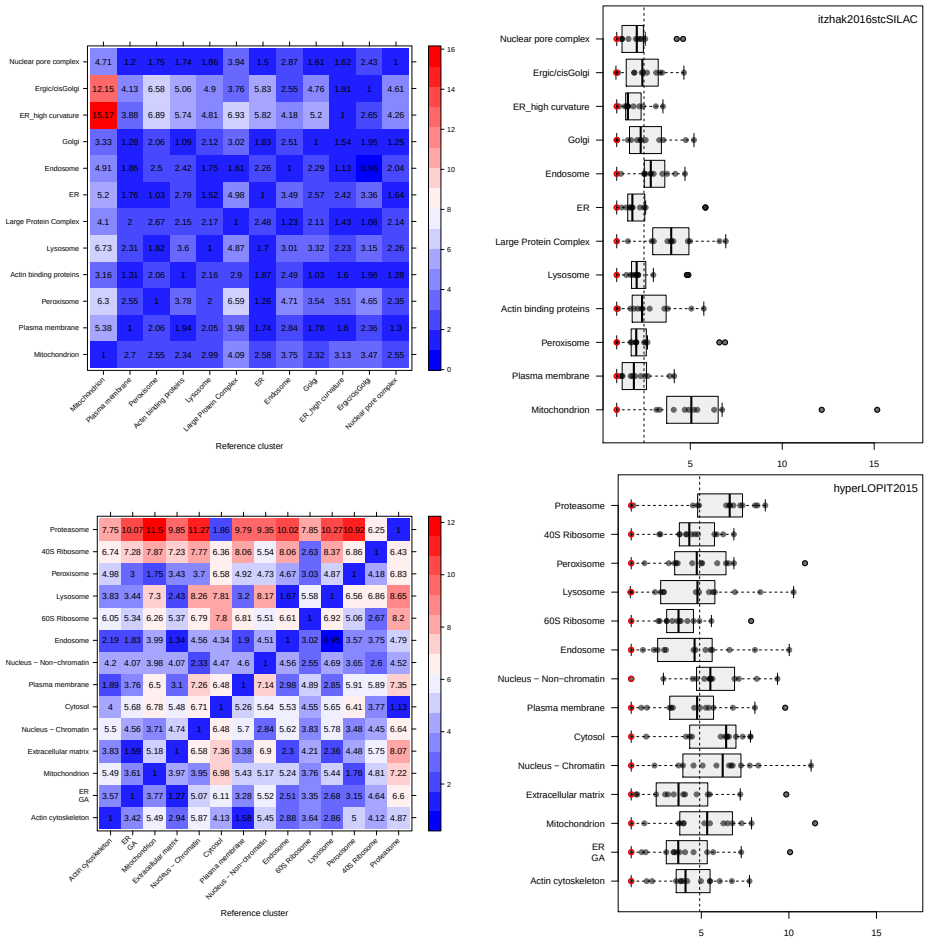

Figure 6: Contrasting quantitative separation assessment between the *itzhak2016stcSILAC* [16] (top) and *hyperLOPIT2015* [4] (bottom) datasets. The dashed vertical lines on the boxplots represent the overall media between cluster distance, 2.48 and 4.91 for *itzhak2016stcSILAC* and *hyperLOPIT2015* respectively.

4 Comparative study

We next apply the quantitative assessment of spatial resolution described in section 3.3 to compare the 29 experiments presented in section 2. On figure 7, we show, for each dataset, a boxplot illustrating the distribution of the global average normalised distances for all spatial clusters. The datasets have been ordered using the experiment-wide median between distance. It is important to always refer back to the original data when considering summarising metrics like these, to put the resolution into context; the density and annotated PCA plots discussed in section 3.2 are provided in figures 11 and 12 and the quantitative assessment boxplots and heatmaps are shown in figures 13 and 14.

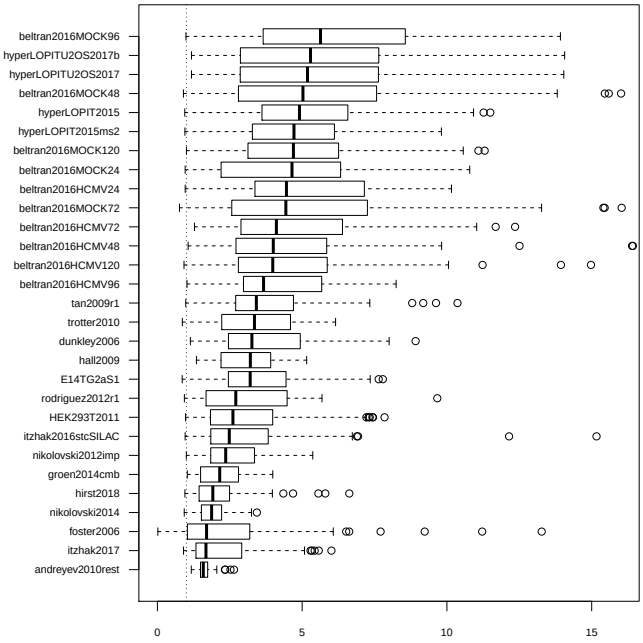

Figure 7: Quantitative separation assessment using experiment-wide normalised distances between cluster distances. The vertical line represents the normalised intra-cluster distance of 1.

The hyperLOPIT experiments *hyperLOPIT2015* and *hyperLOPIT2015ms2* [4] using SPS MS^3 and conventional MS^2 show the best global, experiment-wide resolution. As documented by the authors and illustrated in section 3.2,

the increased quantitation accuracy of the former result in better sub-cellular resolution.

The next set of experiment are *tan2009r1*, *trotter2010*, *dunkley2006*, *hall2009* and *E14TG2aS1*. It is important to highlight that most of datasets (as well as *HEK293T2011*, discussed later) have either been directly re-analysed using a semi-supervised novelty detection algorithm *phenoDisco* [2] (the only exception here being *hall2009*), or, in the case of *trotter2010*, have been annotated using markers based on the *phenoDisco* re-analysis. The novelty detection algorithm, *phenoDisco*, searches for new clusters of unlabelled proteins, using the marker proteins to guide the clustering of unlabelled features. These new clusters, termed *phenotypes*, are then validated by the user for coherence with known sub-cellular niches. This re-analysis has proven successful [2] and has identified previously undetected sub-cellular niches that form tight and well-resolved clusters (see for example ribosomial and trans-Golgi network (TGN) in *dunkley2006*, or proteasome and nucleus in *tan2009r1* to cite only a few), which in turn favour good resolution scores. The *hall2009* dataset is relatively poorly annotated (only 5 sub-cellular clusters, which is the lowest in all test datasets). As long as these few clusters are well separated, poor annotation will not negatively influence the resolution scoring, emphasising the importance of data visualisation (section 3.2).

The next set of experiments that show comparable resolution profiles are *HEK293T2011*, *itzhak2016stcSILAC* and *nikolovski2012imp*. Note that the quantitative separation measurement is robust to questionable marker annotation. For example, the *Large Protein Complex* class defined by the original authors in the *itzhak2016stcSILAC* data could be dropped as it loosely defines many niches and thus lacks resolution. This omission only marginally influences the overall assessment metrics as only the distances to/from that class are affected (i.e. 23 out of 144 distances) and as such it would not change its rank among the test datasets.

As mentioned earlier, the *groen2014cmb* and *nikolovski2014* are targeted experiments, focusing on the trans-Golgi-network and Golgi niches respectively. Such experiments do not aim for the best global resolution, which is reflected by relatively low resolution.

The *foster2006* experiment displays relatively poor separation. This might be due to the relatively high number of missing values (42.4 %). Finally, the *andreyev2010rest* dataset suffers from very broad sub-cellular clusters (compared to separation between clusters).

The PCA plots and QSep heatmaps for all datasets are provided in the appendix, section A.

5 Assessing the resolution metric

In this section, we assess the resolution metric, and how the annotation of the spatial proteomics data influences the metric itself.

We find that the number of classes does not have any effect the resolution assessment scoring. Indeed, dropping any class will result in a sub-sample of normalised inter-cluster distances, with random variations around the overall median inter-cluster distance. On figure 8, we show the distribution of the resolution metrics when removing all possibly combinations of 1 to 3 sub-cellular classes for the *E14TG2aS1* dataset, that displays an average overall resolution, and *hyperLOPIT2015*, that has a highest resolution. In both cases, we see that the number of removed classes does not influence the overall score distributions. When modelling the linear relation between the median scores and the number of removed classes, the slopes are 0.036 and 0.01 respectively.

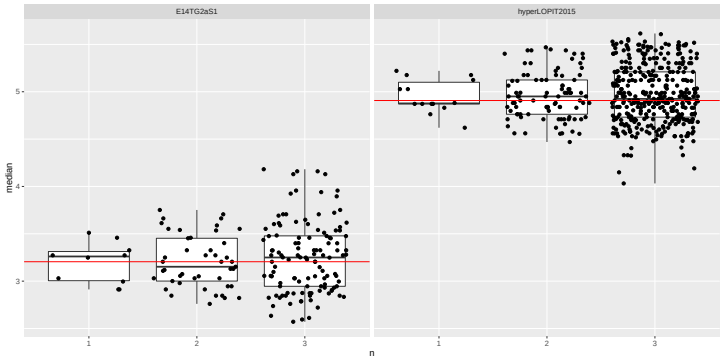

Figure 8: Effect of removing sub-cellular clusters on the resolution metric for the *E14TG2aD1* (left) and *hyperLOPIT2015* experiments (right). Each dot represents a median resolution score for the experimental setting (i.e missing n classes). The horizontal lines represents the median resolution metrics for the complete dataset. Note the overall higher median assessment scores for the better *hyperLOPIT2015* experiment

The definition of marker proteins has of course an effect on the assessment metric. Tighter clusters will result in smaller intra-class distances and,

as a result, in larger normalised inter-class distances. To assess the effect of marker definition, we transferred the marker annotation between the *hyperLOPIT2015* and *itzhak2016stcSILAC* datasets (see PCA plots on figure 9, left) and calculated the quantitative resolution metrics (see boxplots on figure 9, right).

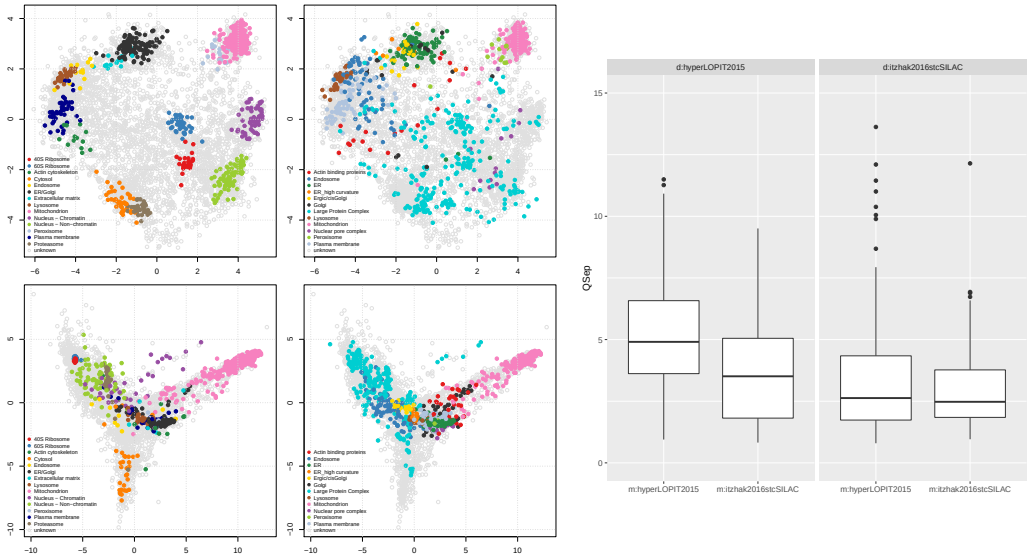

Figure 9: Marker transfer between *hyperLOPIT2015* and *itzhak2016stcSILAC*. On the left, the 4 data/marker combinations are displayed on PCA plots: the top and bottom row contains the *hyperLOPIT2015* and *itzhak2016stcSILAC* data respectively, while the left and right columns display the markers from *hyperLOPIT2015* and *itzhak2016stcSILAC* respectively. On the right, the resolution scores have been calculated for the same markers (along the x axis) data (left and right panels). Note that the y scale has been cut at 15, ignoring outlying scores, to focus on the bulk of the distribution.

As can be seen on figure 9, transferring the *itzhak2016stcSILAC* markers to the *hyperLOPIT2015* dataset has a detrimental effect on the separation (testing the two distributions with a t-test produces a p-value of 5.1×10^{-10}). Conversely, annotating *itzhak2016stcSILAC* with the *hyperLOPIT2015* markers significantly improves its resolution metric (p-value of 1.9×10^{-10}). Comparing both dataset with the *hyperLOPIT2015* marker set favours the resolution of the *hyperLOPIT2015* data (p-value of 2.8×10^{-4})

while using the *itzhak2016stcSILAC* markers with the two datasets substantially reduces their difference in resolution score (p-value of 0.023).

6 Conclusions

In this manuscript, we have described in great detail how to assess and quantify the resolution of spatial proteomics experiments. We have applied dimensionality reduction and visualisation, as well as a simple and intuitive quantitative metric to explore and compare a variety of publicly available spatial proteomics datasets using the annotation provided by the original authors. We have also assessed the resolution metric itself and observed that it was immune to the number of clusters used for its computation and remained consistent to different marker annotation.

The ordering of the quantitative resolution detailed in section 4 should not be taken as absolute. Its main purpose is to provide a guide to compare different experiments. It will be useful for laboratories that do spatial studies on different models and with different fractionation and/or quantitation methods, to assess the impact of these variables (such as, for example hyperLOPIT MS^2 and MS^3). It is also useful to compare separation between different labs, as demonstrated in our comparative study (section 4). We anticipate that it will also prove useful for the researcher wanting to assess the resolution of newly published studies, and put them into a wider context. It is necessary to emphasise that the importance and effect of marker definition on estimating and assessing the resolution of spatial proteomics experiments (section 5) and, of course, the subsequent assignment of proteins to their most likely sub-cellular compartments. Sub-cellular resolution is of course only one aspect of spatial proteomics, albeit am importatn one, that critically determines the reliability of protein assignments to spatial niches as well as the identification of multi- and trans-localisation events.

Finally, we reflect on the implications of this work on the spatial proteomics community, and more generally the cell biology community that relies on protein localisation data. We have assessed dataset spanning 12 years of spatial proteomics. Since 2006, the community has seen many important improvements: tremendous advances in mass spectrometry, improvements in spatial proteomics designs, and considerable breakthroughs in data analysis. One might then wonder whether these benefits have lead to tangible

improvements in resolution over time?

On figure 10, we have ordered the datasets' resolution metric according to their publication year. We can see that a set of recent datasets, including the mouse stem cell [4] and U2OS [26] hyperLOPIT experiments (published in 2016 and 2017 respectively), and a variation thereof, where Jean Beltran et al. [18] (published in 2016), incorporating a temporal component in their experimental design, show a consistent superior resolution.

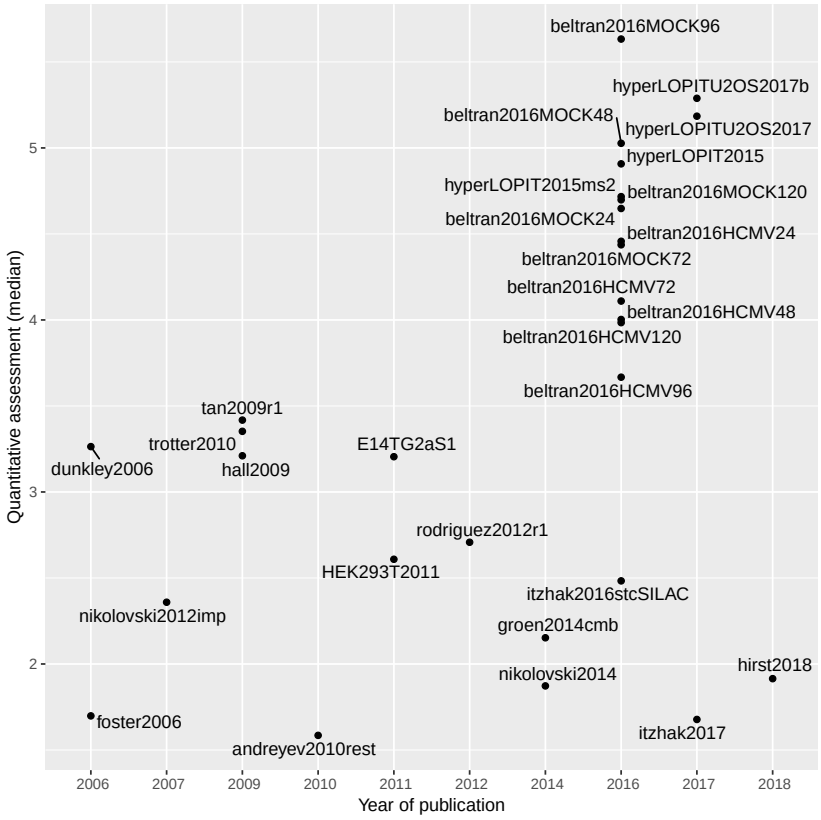

Figure 10: Resolution of spatial proteomics experiments over time. The assigned dates match either the original publication or, when know, the actual date the data was generated. For publications that re-analysed data, the date of the original publication of generation was used. When publications used several datasets, the date of the most recent one was used.

While the definition of sub-cellular resolution, as defined by the QSep measure, is only one aspect of spatial proteomics, one could argue that the

community at large would benefit from a more systematic approach when considering the resolution of spatial proteomics experiments. Indeed, there are various aspects that can be worked on to improve resolution: quantitation accuracy at the mass spectrometry level (see figures 1 and 2 comparing SPS MS^3 and conventional MS^2 for an example), optimisations in sub-cellular fractionation (as exemplified by the substantial improvement obtained by [4]), improved data annotation (see for example figure 9), as well as superior data analysis (for example using semi-supervised learning Breckels et al. [2]).

Maybe there a need for some standardisation, or some general guidelines in assessing spatial proteomics data in the community? Shouldn't the community as a whole aim for collective improvement and some agreement as to what constitutes a good spatial proteomics experiment and a reliable protein sub-cellular assignment? The latter can assessed using improved probabilistic classifiers such as the Bayesian mixture modelling approach proposed by Crook et al. [6]. In this work, we propose the QSep metric to assess the former. Better spatial proteomics data and more reliable interpretation will be of direct benefit to the spatial proteomics researchers themselves, and will increase the trust and reliance of the cell biology community.

Acknowledgements

This work was supported by a BBSRC Strategic Longer and Larger grant (Award BB/L002817/1), a Wellcome Trust Technology Development Grant (Grant number 108441/Z/15/Z) and a BBSRC Tools and resources development grant (Award BB/N023129/1). The authors would like to thank Dr Claire M. Mulvey for helpful comments on the quantitative assessment.

Author contributions

LG conceptualised the method and wrote the initial manuscript draft. LG and LMB developed the QSep code. KSL contributed datasets and feedback. All authors read and approved the manuscript.

Appendices

A Additional figures

This section shows the density and annotated PCA and QSep plots for the 29 datasets showcased in this manuscript.

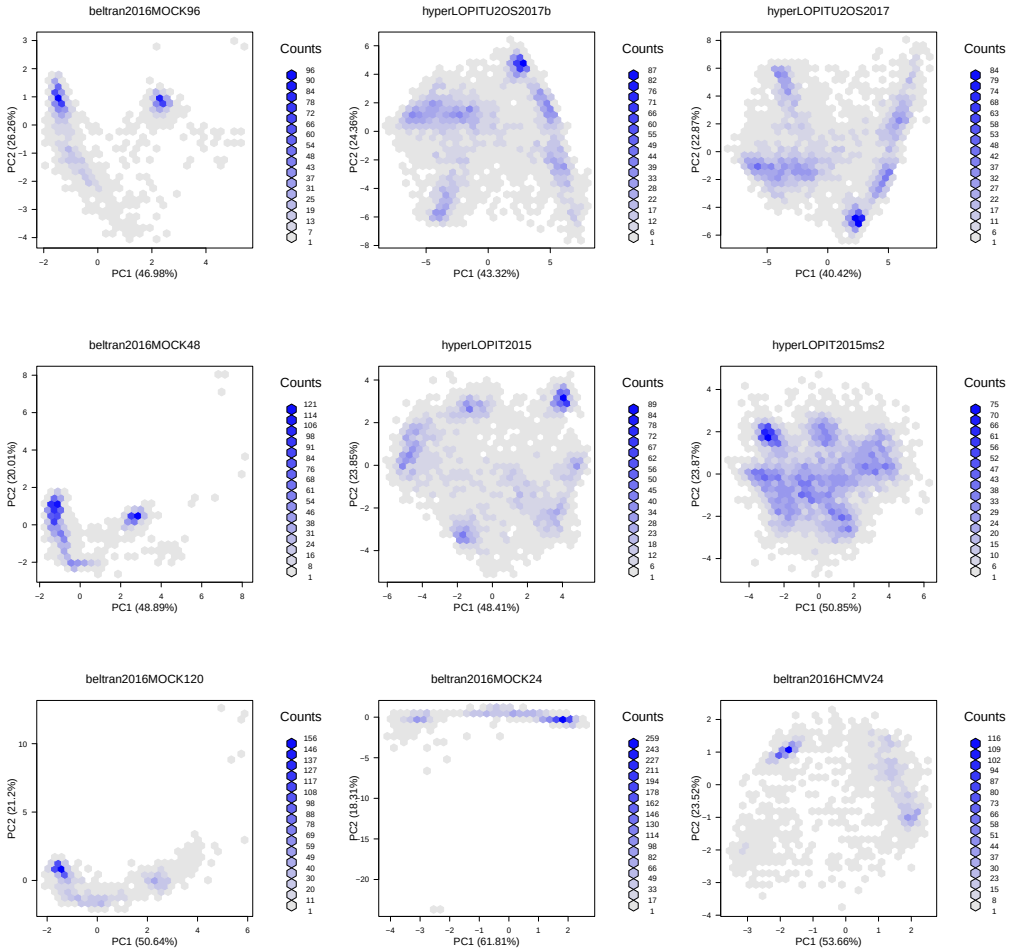

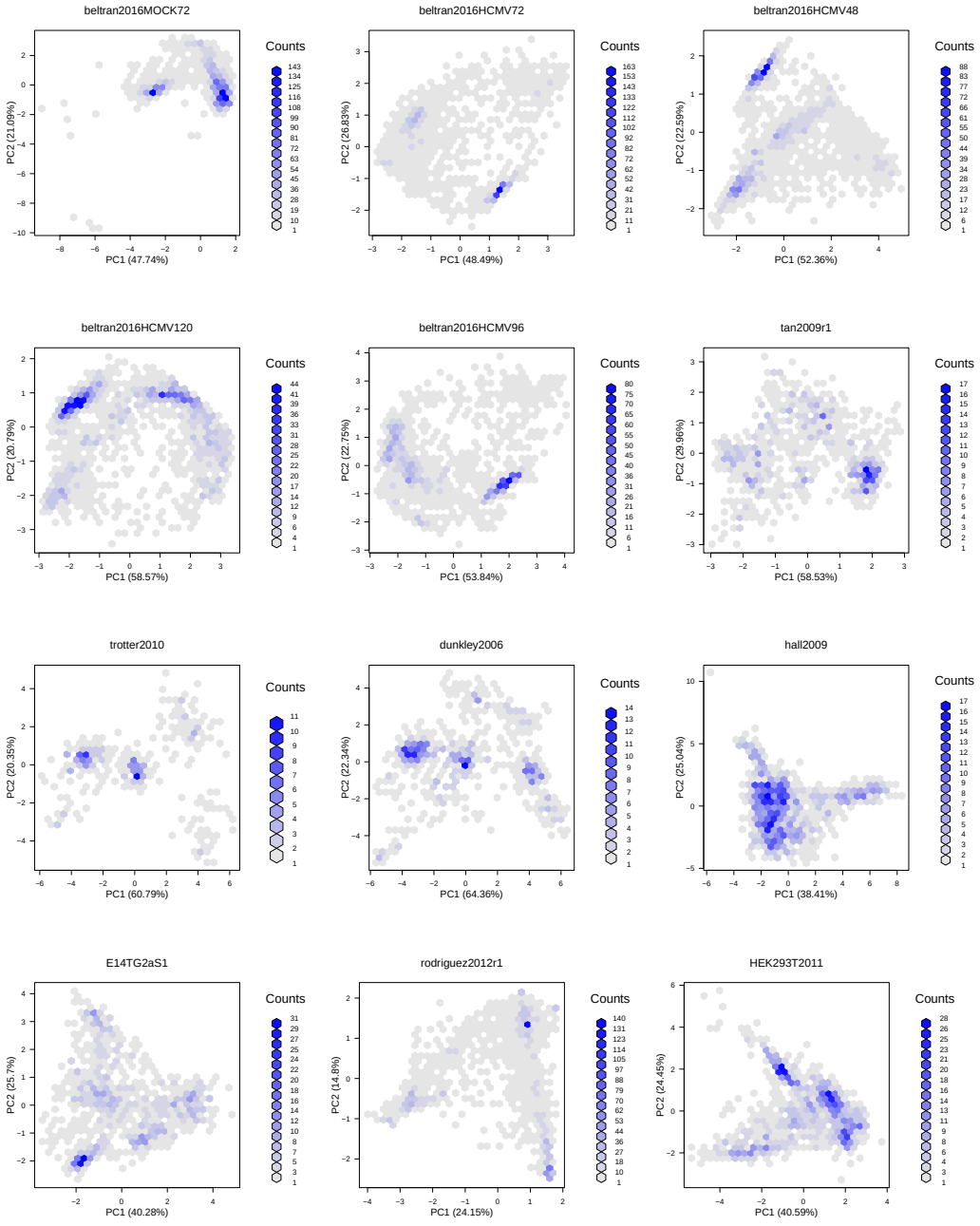
beltran2016MOCK72
PC1 (47.74%)
PC2 (21.09%)
beltran2016HCMV72
PC1 (48.49%)
PC2 (26.83%)
beltran2016HCMV48
PC1 (52.36%)
PC2 (22.59%)
beltran2016HCMV120
PC1 (58.57%)
PC2 (20.79%)
beltran2016HCMV96
PC1 (53.84%)
PC2 (22.75%)
tan2009r1
PC1 (58.53%)
PC2 (29.96%)
trotter2010
PC1 (60.79%)
PC2 (20.35%)
dunkley2006
PC1 (64.36%)
PC2 (22.34%)
hall2009
PC1 (38.41%)
PC2 (25.04%)
E14TG2aS1
PC1 (40.28%)
PC2 (25.7%)
rodriguez2012r1
PC1 (24.15%)
PC2 (14.8%)
HEK293T2011
PC1 (40.59%)
PC2 (24.45%)
Counts

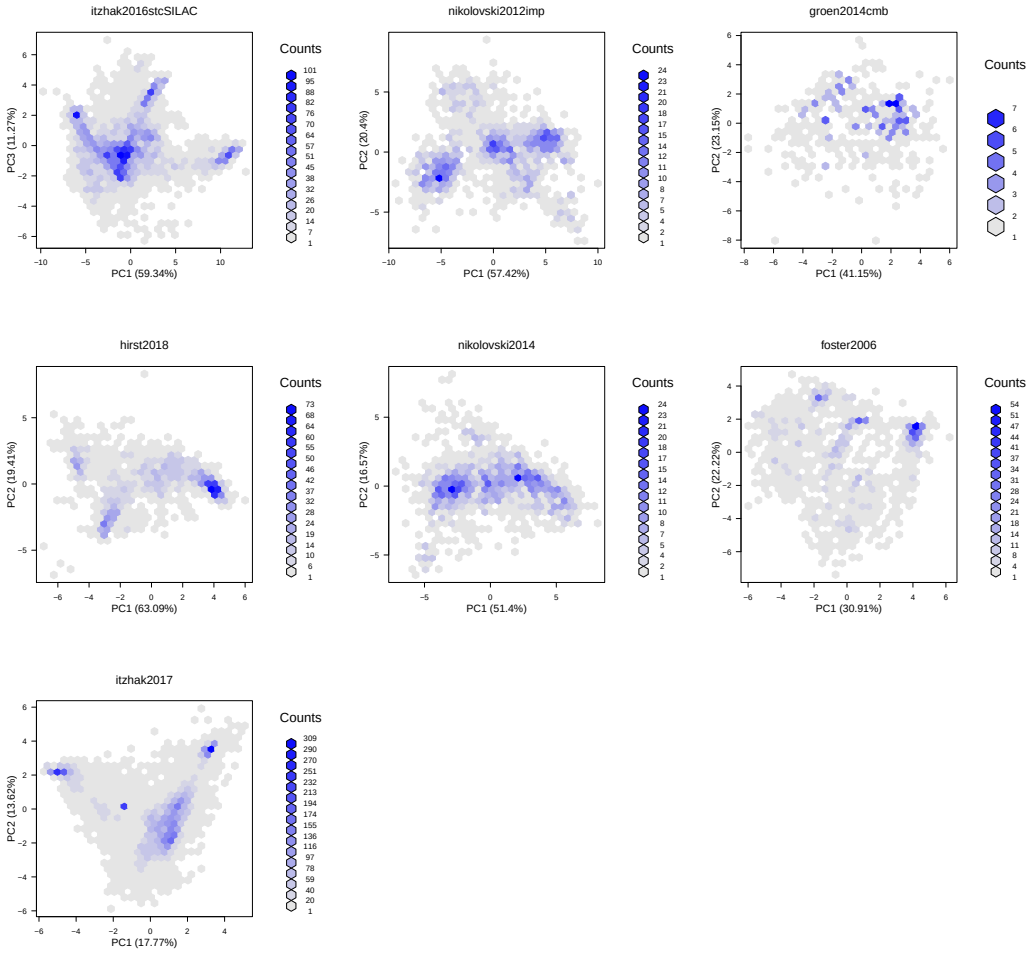

Figure 11: Density PCA plots for the 29 experiments used in this study. PC 1 and 2 were used except for *itzhak2016stcSILAC*, where PC 1 and 3 were used to conform to the original authors figures. The experiments are ordered according to the median average between cluster distance (see figure 7). Figures have been generated using the `plot2D` function from the `pRoloc` package.

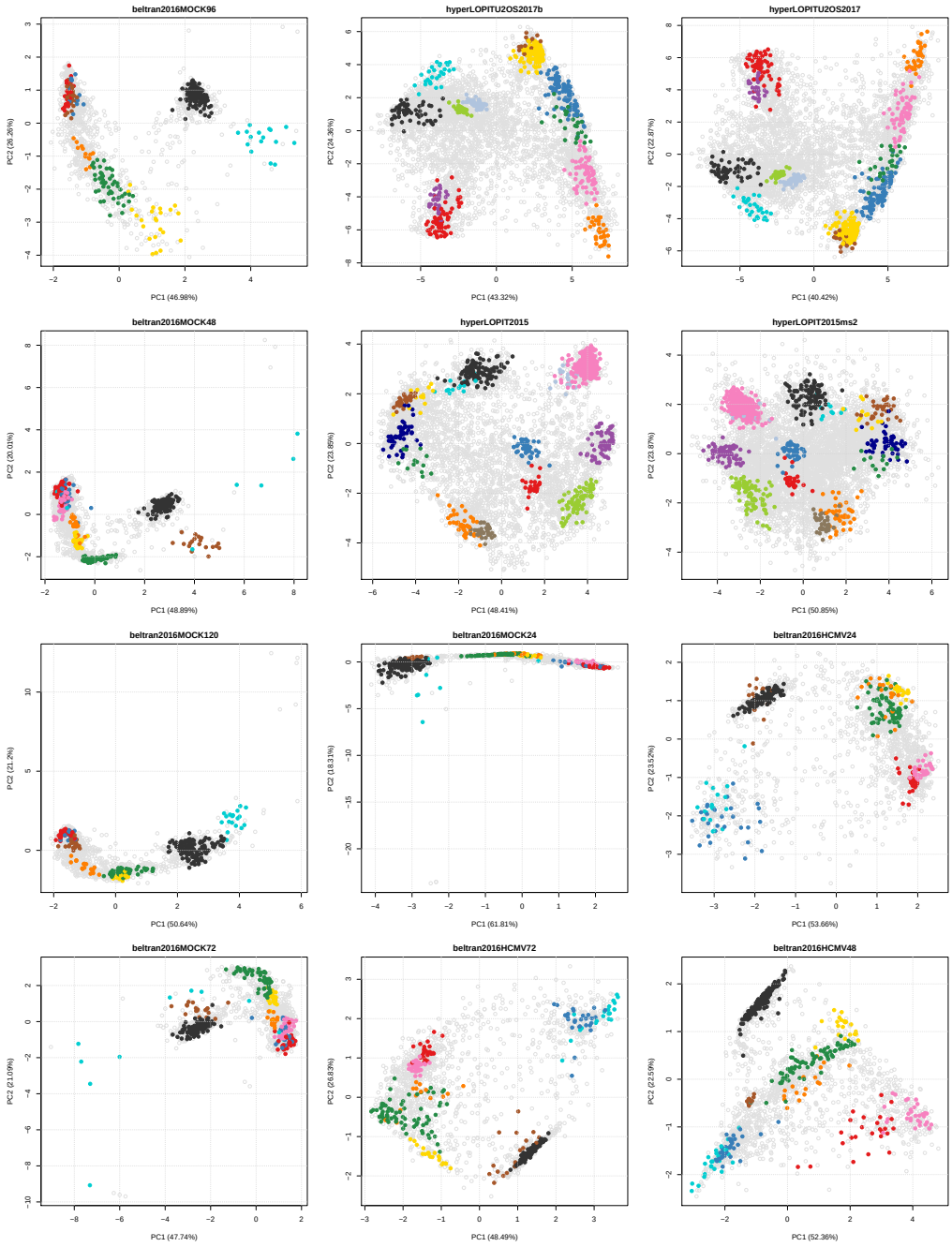
beltran2016MOCK96
PC1 (46.98%)
PC2 (26.26%)
hyperLOPITU2OS2017b
PC1 (43.32%)
PC2 (24.36%)
hyperLOPITU2OS2017
PC1 (40.42%)
PC2 (22.87%)
beltran2016MOCK48
PC1 (48.89%)
PC2 (20.01%)
hyperLOPIT2015
PC1 (48.41%)
PC2 (23.85%)
hyperLOPIT2015ms2
PC1 (50.85%)
PC2 (23.87%)
beltran2016MOCK120
PC1 (50.64%)
PC2 (21.2%)
beltran2016MOCK24
PC1 (61.81%)
PC2 (18.31%)
beltran2016HCMV24
PC1 (53.66%)
PC2 (23.52%)
beltran2016MOCK72
PC1 (47.74%)
PC2 (21.09%)
beltran2016HCMV72
PC1 (48.49%)
PC2 (26.83%)
beltran2016HCMV48
PC1 (52.36%)
PC2 (22.59%)

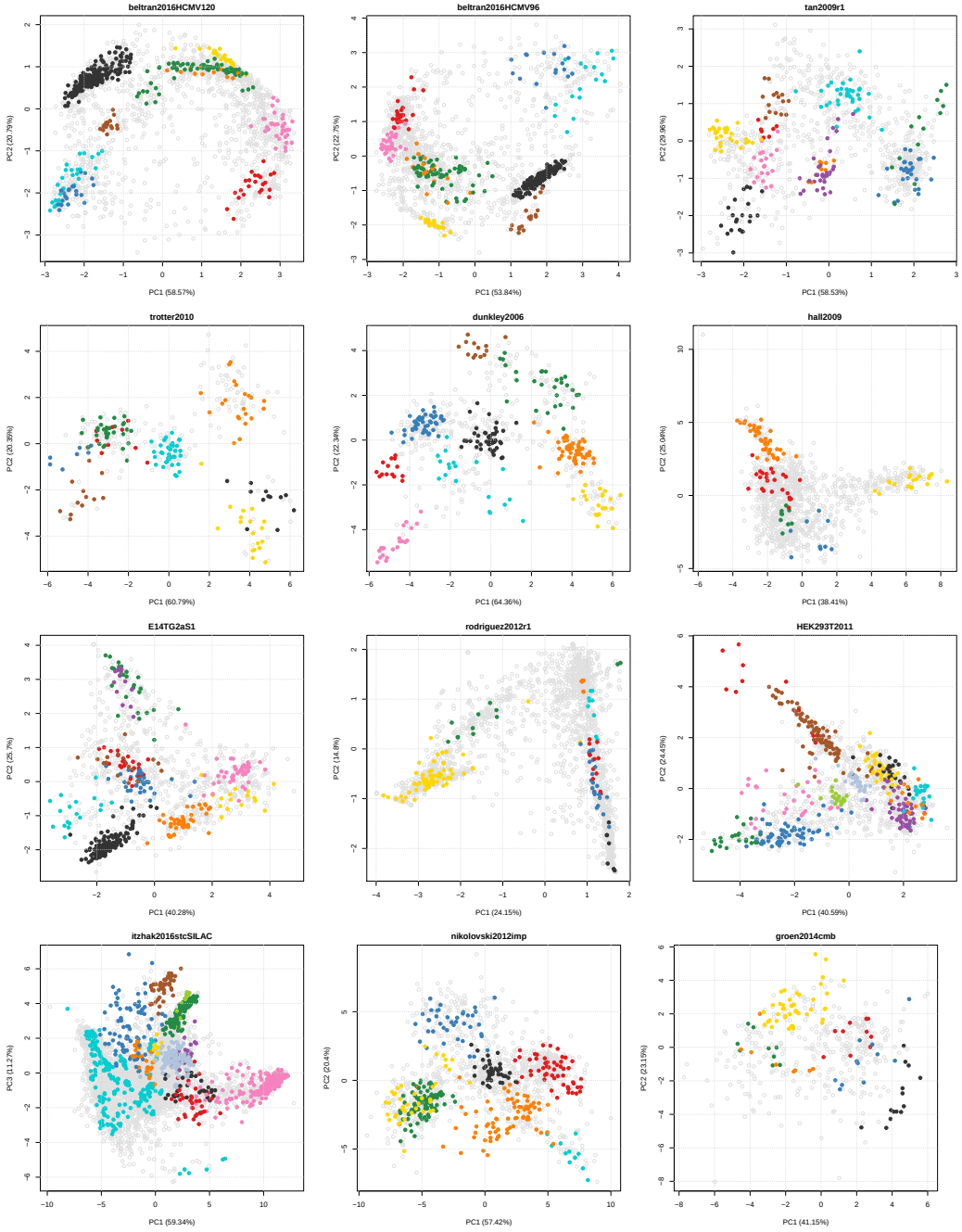
beltran2016HCMV120
PC1 (58.57%)
PC2 (20.79%)
beltran2016HCMV96
PC1 (53.84%)
PC2 (22.75%)
tan2009r1
PC1 (58.53%)
PC2 (29.96%)
trotter2010
PC1 (60.79%)
PC2 (20.39%)
dunkley2006
PC1 (64.36%)
PC2 (22.34%)
hall2009
PC1 (38.41%)
PC2 (25.04%)
E14TG2aS1
PC1 (40.28%)
PC2 (25.7%)
rodriguez2012r1
PC1 (24.15%)
PC2 (14.8%)
HEK293T2011
PC1 (40.59%)
PC2 (24.49%)
itzhak2016stcSILAC
PC1 (59.34%)
PC3 (12.7%)
nikolovski2012imp
PC1 (57.42%)
PC2 (20.4%)
groen2014cmb
PC1 (41.15%)
PC2 (23.19%)

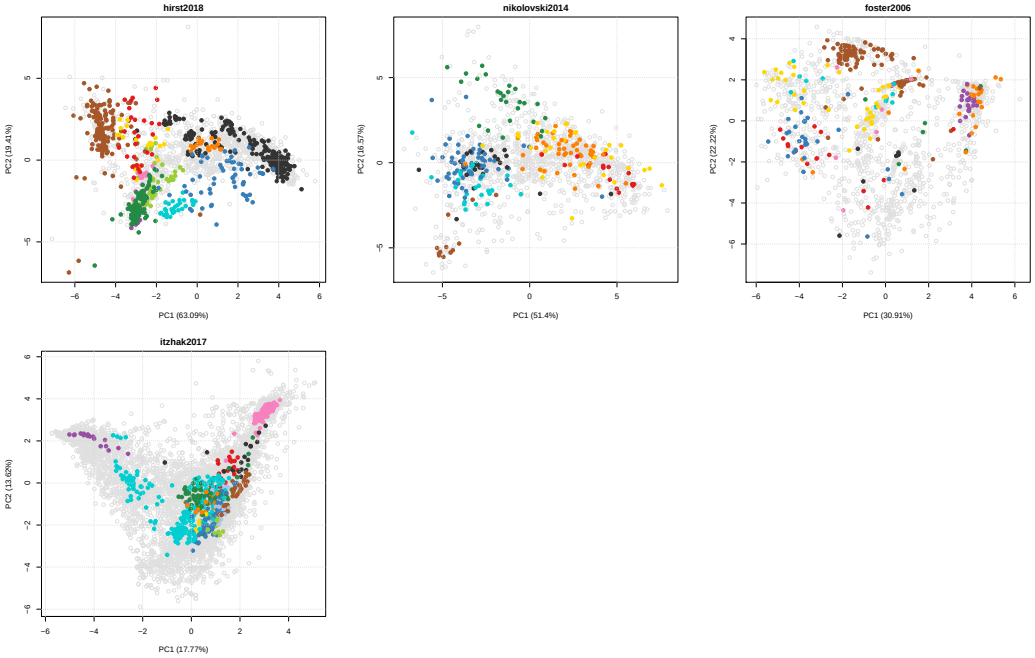

Figure 12: PCA plots for the 29 experiments used in this study. PC 1 and 2 were used except for *itzhak2016stcSILAC*, where PC 1 and 3 were used to conform to the original authors figures. The experiments are ordered according to the median average between cluster distance (see figure 7). The percentage of variance explained along the 2 PCs on the plots can be found in table 1. Figures have been generated using the `plot2D` function from the `pRoloc` package.

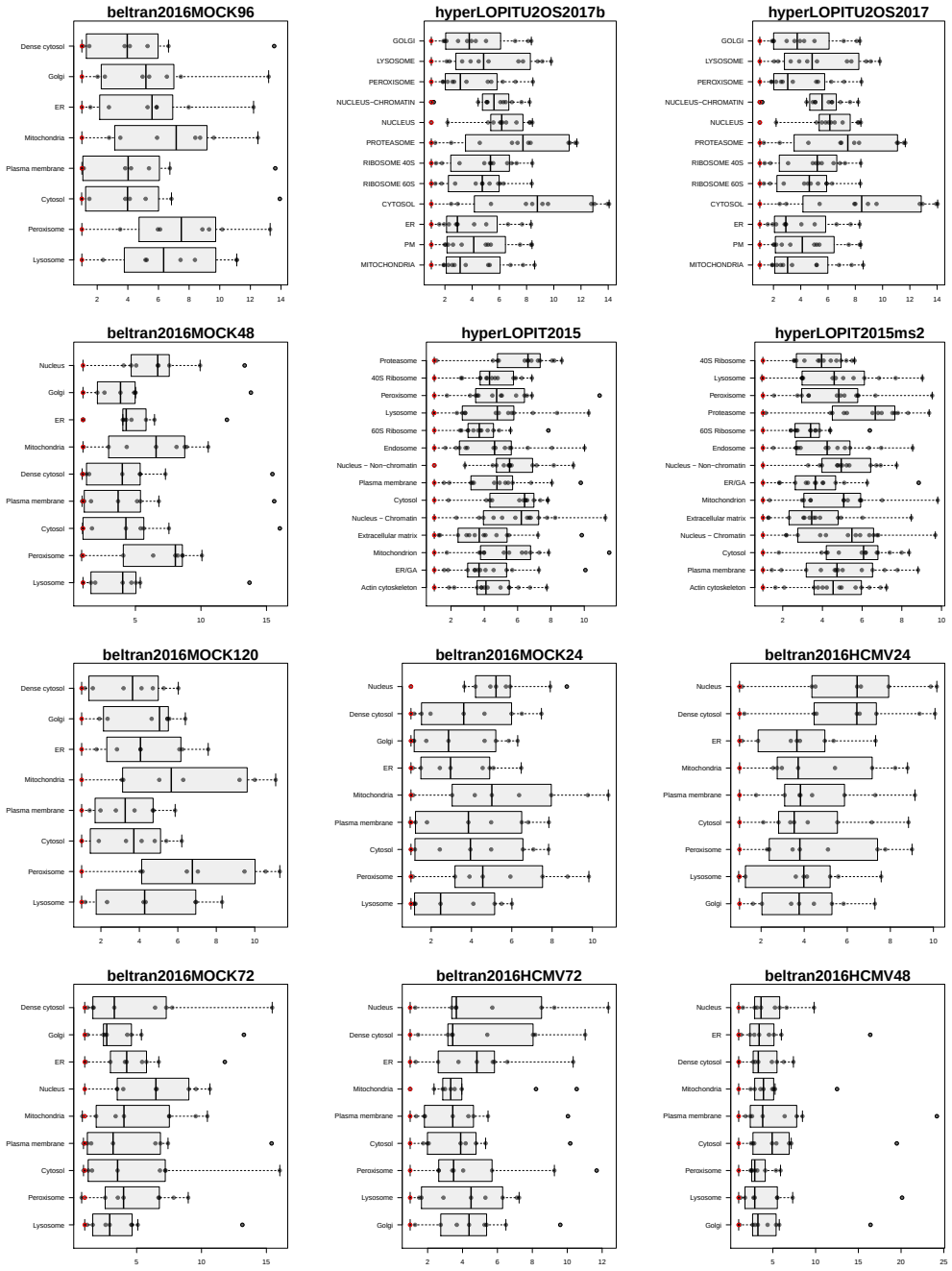
beltran2016MOCK96
Dense cytosol
Golgi
ER
Mitochondria
Plasma membrane
Cytosol
Peroxisome
Lysosome
hyperLOPITU2OS2017b
GOLGI
LYSOSOME
PEROXISOME
NUCLEUS−CHROMATIN
NUCLEUS
PROTEASOME
RIBOSOME 40S
RIBOSOME 60S
CYTOSOL
ER
PM
MITOCHONDRIA
hyperLOPITU2OS2017
beltran2016MOCK48
Nucleus
hyperLOPIT2015
Proteasome
40S Ribosome
Lysosome
60S Ribosome
Endosome
Nucleus − Non−chromatin
Nucleus − Chromatin
Extracellular matrix
Mitochondrion
ER/GA
Actin cytoskeleton
hyperLOPIT2015ms2
ER/GA
beltran2016MOCK120
beltran2016MOCK24
beltran2016HCMV24
beltran2016MOCK72
beltran2016HCMV72
beltran2016HCMV48

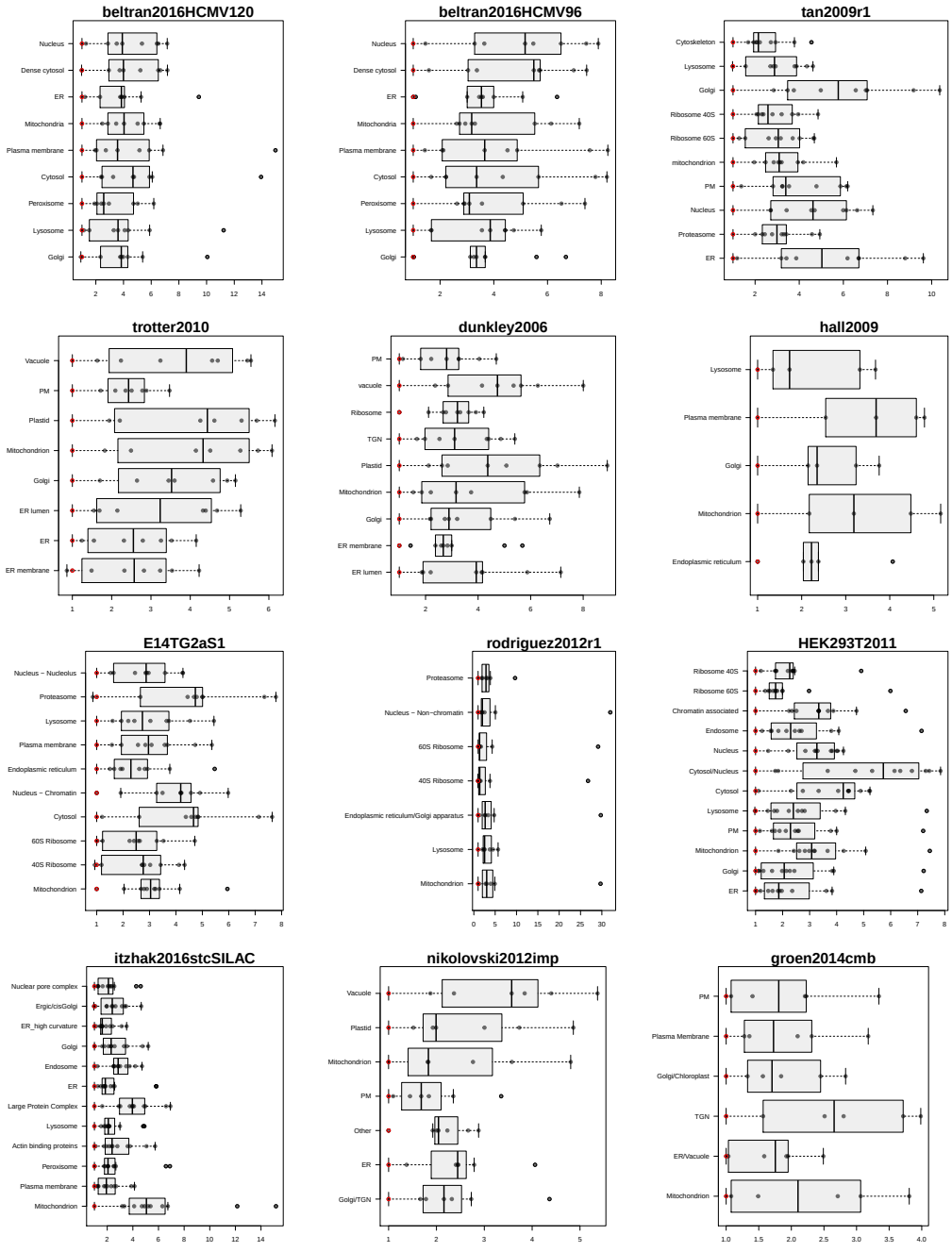
beltran2016HCMV120
Nucleus
Dense cytosol
ER
Mitochondria
Plasma membrane
Cytosol
Peroxisome
Lysosome
Golgi
beltran2016HCMV96
Nucleus
Dense cytosol
ER
Mitochondria
Plasma membrane
Cytosol
Peroxisome
Lysosome
Golgi
tan2009r1
Cytoskeleton
Lysosome
Golgi
Ribosome 40S
Ribosome 60S
mitochondrion
PM
Nucleus
Proteasome
ER
trotter2010
Vacuole
PM
Plastid
Mitochondrion
Golgi
ER lumen
ER
ER membrane
dunkley2006
PM
vacuole
Ribosome
TGN
Plastid
Mitochondrion
Golgi
ER membrane
ER lumen
hall2009
Lysosome
Plasma membrane
Golgi
Mitochondrion
Endoplasmic reticulum
E14TG2aS1
Nucleus − Nucleolus
Proteasome
Lysosome
Plasma membrane
Endoplasmic reticulum
Nucleus − Chromatin
Cytosol
60S Ribosome
40S Ribosome
Mitochondrion
rodriguez2012r1
Proteasome
Nucleus − Non−chromatin
60S Ribosome
40S Ribosome
Endoplasmic reticulum/Golgi apparatus
Lysosome
Mitochondrion
HEK293T2011
Ribosome 40S
Ribosome 60S
Chromatin associated
Endosome
Nucleus
Cytosol/Nucleus
Cytosol
Lysosome
PM
Mitochondrion
Golgi
ER
itzhak2016stcSILAC
Nuclear pore complex
Ergic/cisGolgi
ER_high curvature
Golgi
Endosome
ER
Large Protein Complex
Lysosome
Actin binding proteins
Peroxisome
Plasma membrane
Mitochondrion
nikolovski2012imp
Vacuole
Plastid
Mitochondrion
PM
Other
ER
Golgi/TGN
groen2014cmb
PM
Plasma Membrane
Golgi/Chloroplast
TGN
ER/Vacuole
Mitochondrion

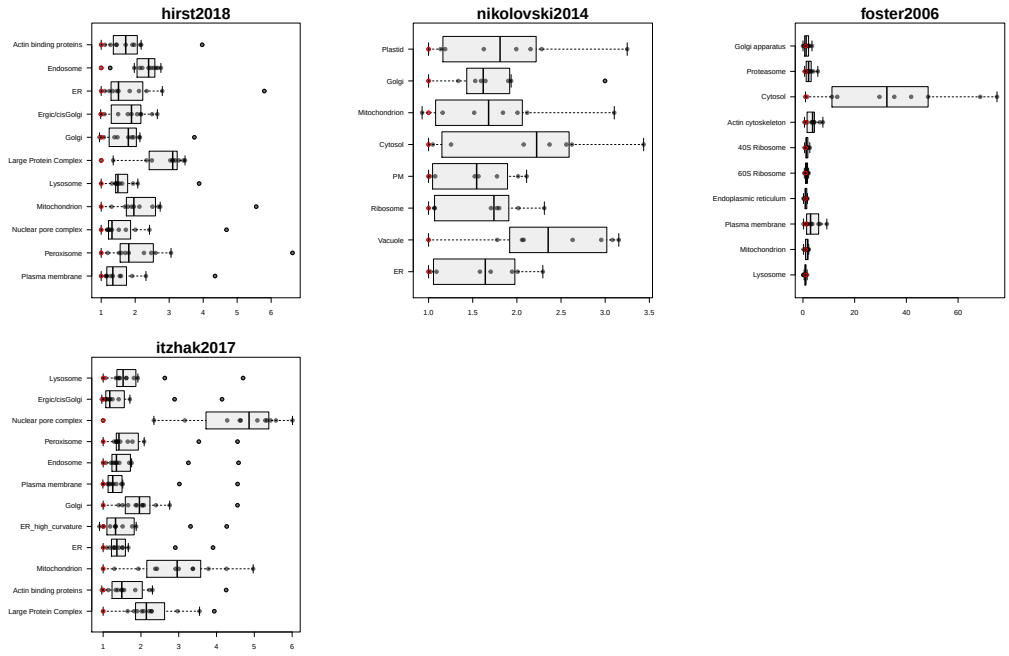

Figure 13: Quantitative separation boxplot for the 29 experiments used in this study. The experiments are ordered according to the median average between cluster distance (see figure 7).

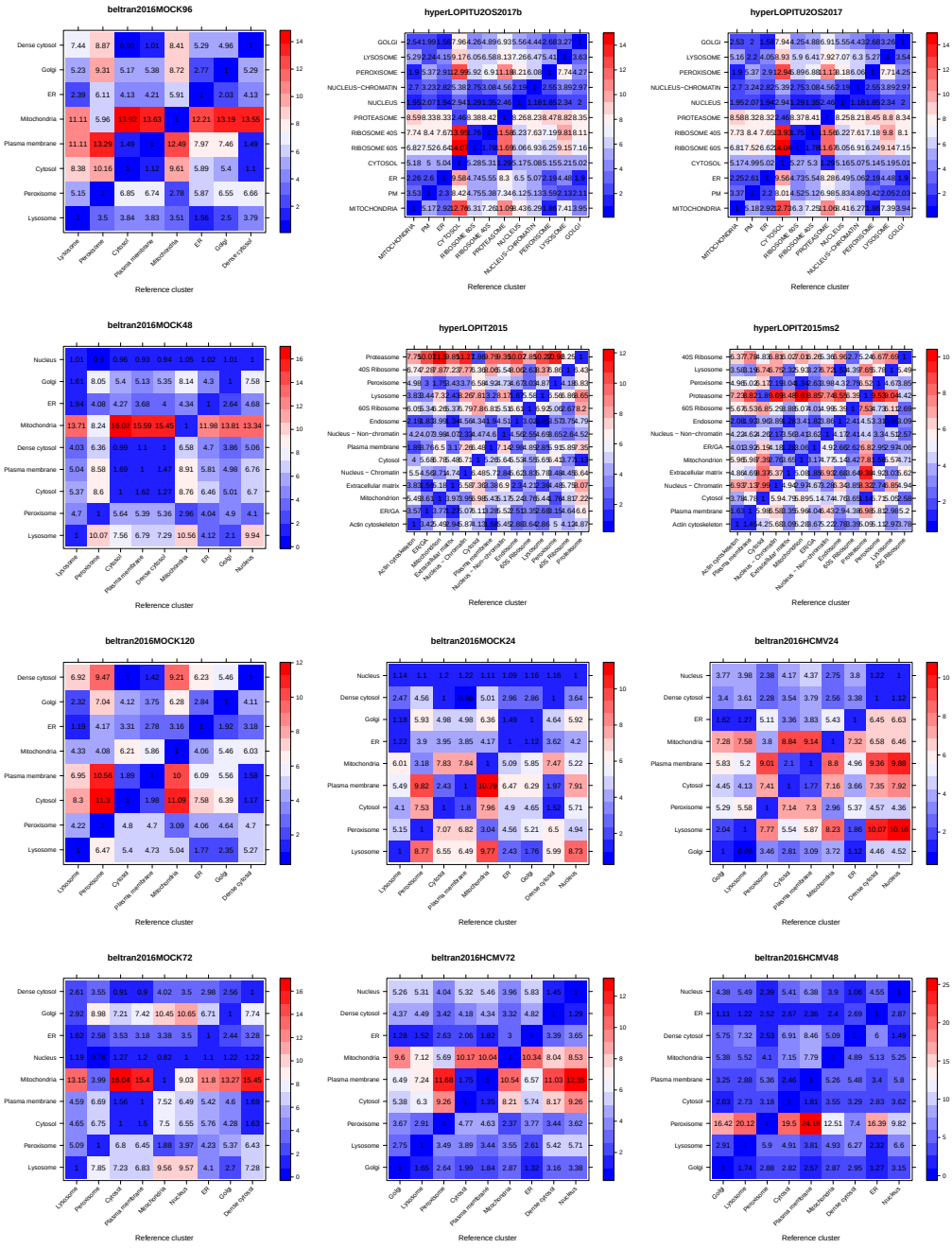
beltran2016MOCK96
hyperLOPITU2OS2017b
hyperLOPITU2OS2017
beltran2016MOCK48
hyperLOPIT2015
hyperLOPIT2015ms2
beltran2016MOCK120
beltran2016MOCK24
beltran2016HCMV24
beltran2016MOCK72
beltran2016HCMV72
beltran2016HCMV48
Reference cluster

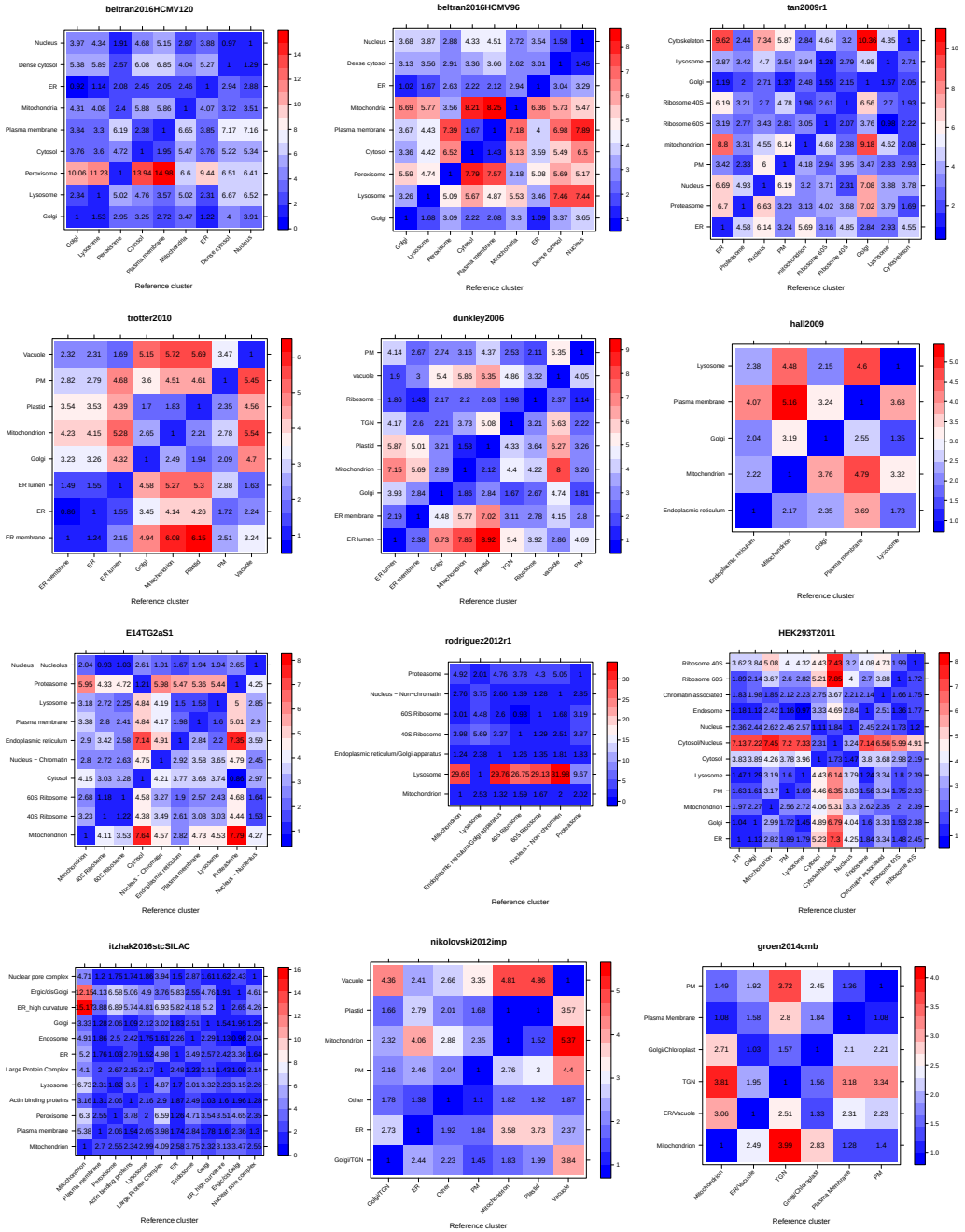
beltran2016HCMV120
Nucleus
Dense cytosol
ER
Mitochondria
Plasma membrane
Cytosol
Peroxisome
Lysosome
Golgi
Golgi
Lysosome
Peroxisome
Cytosol
Plasma membrane
Mitochondria
ER
Dense cytosol
Nucleus
Reference cluster
beltran2016HCMV96
Nucleus
Dense cytosol
ER
Mitochondria
Plasma membrane
Cytosol
Peroxisome
Lysosome
Golgi
Golgi
Lysosome
Peroxisome
Cytosol
Plasma membrane
Mitochondria
ER
Dense cytosol
Nucleus
Reference cluster
tan2009r1
Cytoskeleton
Lysosome
Golgi
Ribosome 40S
Ribosome 60S
mitochondrion
PM
Nucleus
Proteasome
ER
ER
Proteasome
Nucleus
PM
mitochondrion
Ribosome 60S
Ribosome 40S
Golgi
Lysosome
Cytoskeleton
Reference cluster
trotter2010
Vacuole
PM
Plastid
Mitochondrion
Golgi
ER lumen
ER
ER membrane
ER membrane
ER
ER lumen
Golgi
Mitochondrion
Plastid
PM
Vacuole
Reference cluster
dunkley2006
PM
vacuole
Ribosome
TGN
Plastid
Mitochondrion
Golgi
ER membrane
ER lumen
ER lumen
ER membrane
Golgi
Mitochondrion
Plastid
TGN
Ribosome
vacuole
PM
Reference cluster
hall2009
Lysosome
Plasma membrane
Golgi
Mitochondrion
Endoplasmic reticulum
Endoplasmic reticulum
Mitochondrion
Golgi
Plasma membrane
Lysosome
Reference cluster
E14TG2aS1
Nucleus − Nucleolus
Proteasome
Lysosome
Plasma membrane
Endoplasmic reticulum
Nucleus − Chromatin
Cytosol
60S Ribosome
40S Ribosome
Mitochondrion
Mitochondrion
40S Ribosome
60S Ribosome
Cytosol
Nucleus − Chromatin
Endoplasmic reticulum
Plasma membrane
Lysosome
Proteasome
Nucleus − Nucleolus
Reference cluster
rodriguez2012r1
Proteasome
Nucleus − Non−chromatin
60S Ribosome
40S Ribosome
Endoplasmic reticulum/Golgi apparatus
Lysosome
Mitochondrion
Mitochondrion
Lysosome
Endoplasmic reticulum/Golgi apparatus
40S Ribosome
60S Ribosome
Nucleus − Non−chromatin
Proteasome
Reference cluster
HEK293T2011
Ribosome 40S
Ribosome 60S
Chromatin associated
Endosome
Nucleus
Cytosol/Nucleus
Cytosol
Lysosome
PM
Mitochondrion
Golgi
ER
ER
Golgi
Mitochondrion
PM
Lysosome
Cytosol
Cytosol/Nucleus
Nucleus
Endosome
Chromatin associated
Ribosome 60S
Ribosome 40S
Reference cluster
itzhak2016stcSILAC
Nuclear pore complex
Ergic/cisGolgi
ER_high curvature
Golgi
Endosome
ER
Large Protein Complex
Lysosome
Actin binding proteins
Peroxisome
Plasma membrane
Mitochondrion
Mitochondrion
Plasma membrane
Peroxisome
Actin binding proteins
Lysosome
Large Protein Complex
ER
Endosome
Golgi
ER_high curvature
Ergic/cisGolgi
Nuclear pore complex
Reference cluster
nikolovski2012imp
Vacuole
Plastid
Mitochondrion
PM
Other
ER
Golgi/TGN
Golgi/TGN
ER
Other
PM
Mitochondrion
Plastid
Vacuole
Reference cluster
groen2014cmb
PM
Plasma Membrane
Golgi/Chloroplast
TGN
ER/Vacuole
Mitochondrion
Mitochondrion
ER/Vacuole
TGN
Golgi/Chloroplast
Plasma Membrane
PM
Reference cluster

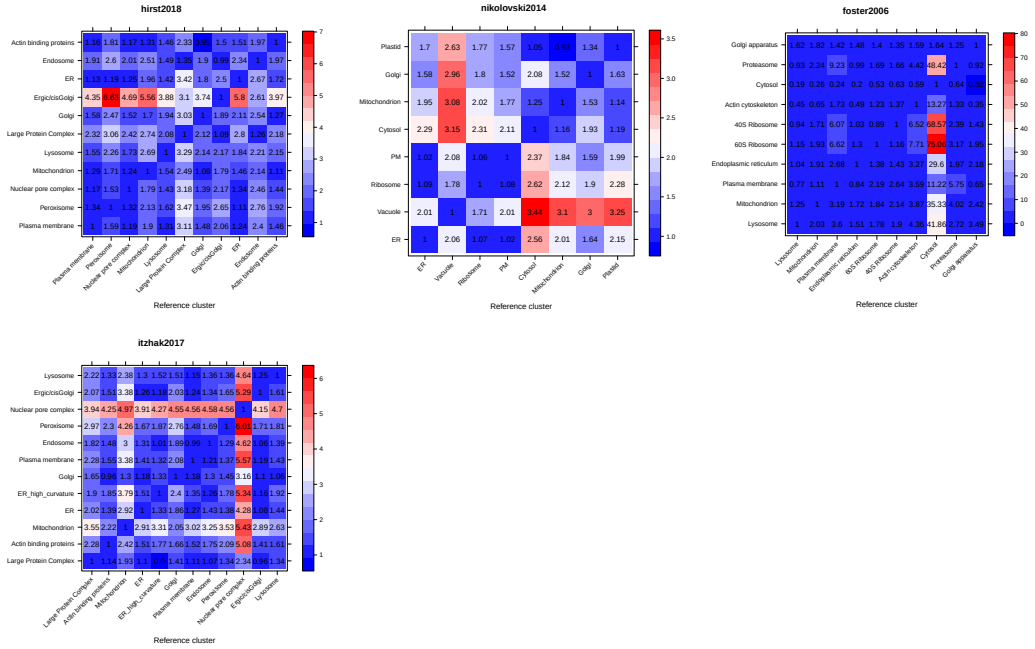

Figure 14: Quantitative separation heatmaps for the 29 experiments used in this study. The experiments are ordered according to the median average between cluster distance (see figure 7).

B Session information

The software and versions used to produce this document are summarised below. The source of this document enabling to reproduce all results and figures is available in the source of this document in the public manuscript repository [9] available at `https://github.com/lgatto/QSep-manuscript/`.

- R Under development (unstable) (2018-04-02 r74505), `x86_64-pc-linux-gnu`
- Running under: `Ubuntu 14.04.5 LTS`
- Matrix products: default
- BLAS: `/usr/lib/atlas-base/atlas/libblas.so.3.0`
- LAPACK: `/usr/lib/lapack/liblapack.so.3.0`
- Base packages: base, datasets, graphics, grDevices, methods, parallel, stats, stats4, utils
- Other packages: annotate 1.58.0, AnnotationDbi 1.42.1, Biobase 2.40.0, BiocGenerics 0.26.0, BiocParallel 1.14.2, cluster 2.0.7-1, ggplot2 3.0.0, ggrepel 0.8.0, hexbin 1.27.2, IRanges 2.14.10, MLInterfaces 1.60.1, MSnbase 2.7.3, mzR 2.15.2, pRoloc 1.21.7, pRolocdata 1.18.0, ProtGenerics 1.12.0, Rcpp 0.12.18, S4Vectors 0.18.3, XML 3.98-1.12, xtable 1.8-2
- Loaded via a namespace (and not attached): abind 1.4-5, affy 1.58.0, affyio 1.50.0, assertthat 0.2.0, backports 1.1.2, base64enc 0.1-3, bindr 0.1.1, bindrcpp 0.2.2, BiocInstaller 1.30.0, biomaRt 2.36.1, bit 1.1-14, bit64 0.9-7, bitops 1.0-6, blob 1.1.1, broom 0.5.0, caret 6.0-80, class 7.3-14, coda 0.19-1, codetools 0.2-15, colorspace 1.3-2, compiler 3.6.0, crayon 1.3.4, crosstalk 1.0.0, CVST 0.2-2, DBI 1.0.0, ddalpha 1.3.4, dendextend 1.8.0, DEoptimR 1.0-8, digest 0.6.15, dimRed 0.1.0, diptest 0.75-7, doParallel 1.0.11, dplyr 0.7.6, DRR 0.0.3, e1071 1.6-8, evaluate 0.11, flexmix 2.3-14, FNN 1.1, foreach 1.4.4, fpc 2.1-11.1, gbm 2.1.3, gdata 2.18.0, genefilter 1.62.0, geometry 0.3-6, ggvis 0.4.3, glue 1.3.0, gower 0.1.2, grid 3.6.0, gridExtra 2.3, gtable 0.2.0, gtools 3.8.1,

highr 0.7, hms 0.4.2, htmltools 0.3.6, htmlwidgets 1.2, httpuv 1.4.5, httr 1.3.1, hwriter 1.3.2, igraph 1.2.1, impute 1.54.0, ipred 0.9-6, iterators 1.0.10, kernlab 0.9-26, knitr 1.20, labeling 0.3, LaplacesDemon 16.1.1, later 0.7.3, lattice 0.20-35, lava 1.6.2, lazyeval 0.2.1, limma 3.36.2, lpSolve 5.6.13, lubridate 1.7.4, magic 1.5-8, magrittr 1.5, MALDIquant 1.18, MASS 7.3-50, Matrix 1.2-14, mclust 5.4.1, memoise 1.1.0, mime 0.5, mixtools 1.1.0, mlbench 2.1-1, ModelMetrics 1.1.0, modeltools 0.2-22, munsell 0.5.0, mvtnorm 1.0-8, mzID 1.18.0, nlme 3.1-137, nnet 7.3-12, pcaMethods 1.72.0, pillar 1.3.0, pkgconfig 2.0.1, pls 2.6-0, plyr 1.8.4, prabclus 2.2-6, preprocessCore 1.42.0, prettyunits 1.0.2, prodlim 2018.04.18, progress 1.2.0, promises 1.0.1, proxy 0.4-22, purrr 0.2.5, R6 2.2.2, randomForest 4.6-14, RColorBrewer 1.1-2, RcppRoll 0.3.0, RCurl 1.95-4.11, rda 1.0.2-2.1, recipes 0.1.3, reshape2 1.4.3, rlang 0.2.1, robustbase 0.93-1.1, rpart 4.1-13, RSQLite 2.1.1, sampling 2.8, scales 0.5.0, segmented 0.5-3.0, sfsmisc 1.1-2, shiny 1.1.0, splines 3.6.0, stringi 1.2.4, stringr 1.3.1, survival 2.42-4, threejs 0.3.1, tibble 1.4.2, tidyr 0.8.1, tidyselect 0.2.4, timeDate 3043.102, tools 3.6.0, trimcluster 0.1-2.1, viridis 0.5.1, viridisLite 0.3.0, vsn 3.48.1, whisker 0.3-2, withr 2.1.2, zlibbioc 1.26.0

References

[1] A Y Andreyev, Z Shen, Z Guan, A Ryan, E Fahy, S Subramaniam, C R Raetz, S Briggs, and E A Dennis. Application of proteomic marker ensembles to subcellular organelle identification. *Mol Cell Proteomics*, 9(2):388–402, Feb 2010. doi: 10.1074/mcp.M900432-MCP200.

[2] L M Breckels, L Gatto, A Christoforou, A J Groen, K S Lilley, and M W Trotter. The effect of organelle discovery upon sub-cellular protein localisation. *J Proteomics*, 88:129–40, Aug 2013. doi: 10.1016/j.jprot.2013.02.019.

[3] L M Breckels, S B Holden, D Wojnar, C M Mulvey, A Christoforou, A Groen, M W Trotter, O Kohlbacher, K S Lilley, and L Gatto. Learning from heterogeneous data sources: An application in spatial proteomics. *PLoS Comput Biol*, 12(5):e1004920, May 2016. doi: 10.1371/journal.pcbi.1004920.

[4] A Christoforou, C M Mulvey, L M Breckels, A Geladaki, T Hurrell, P C Hayward, T Naake, L Gatto, R Viner, A Martinez Arias, and K S Lilley. A draft map of the mouse pluripotent stem cell spatial proteome. *Nat Commun*, 7:8992, 2016. doi: 10.1038/ncomms9992.

[5] N A Cody, C Iampietro, and E Lcuyer. The many functions of mRNA localization during normal development and disease: from pillar to post. *Wiley Interdiscip Rev Dev Biol*, 2(6):781–96, 2013. doi: 10.1002/wdev.113.

[6] Oliver M Crook, Claire M Mulvey, Paul D. W. Kirk, Kathryn S Lilley, and Laurent Gatto. A bayesian mixture modelling approach for spatial proteomics. *bioRxiv*, 2018. doi: 10.1101/282269. URL `https://www.biorxiv.org/content/early/2018/05/23/282269`.

[7] T P. J. Dunkley, S Hester, I P Shadforth, J Runions, T Weimar, S L Hanton, J L Griffin, C Bessant, F Brandizzi, C Hawes, R B Watson, P Dupree, and K S Lilley. Mapping the arabidopsis organelle proteome. *Proc Natl Acad Sci USA*, 103(17):6518–6523, Apr 2006. doi: 10.1073/pnas.0506958103.

[8] L J Foster, C L de Hoog, Y Zhang, Y Zhang, X Xie, V K. Mootha, and M Mann. A mammalian organelle map by protein correlation profiling. *Cell*, 125(1):187–199, Apr 2006. doi: 10.1016/j.cell.2006.03.022.

[9] L Gatto. Assessing sub-cellular resolution in spatial proteomics experiments. `https://github.com/lgatto/QSep-manuscript/`, 2018.

[10] L Gatto, J A Vizcaíno, H Hermjakob, W Huber, and K S Lilley. Organelle proteomics experimental designs and analysis. *Proteomics*, 10 (22):3957–69, Nov 2010. doi: 10.1002/pmic.201000244.

[11] L Gatto, L M Breckels, T Burger, D J Nightingale, A J Groen, C Campbell, N Nikolovski, C M Mulvey, A Christoforou, M Ferro, and K S Lilley. A foundation for reliable spatial proteomics data analysis. *Mol Cell Proteomics*, 13(8):1937–52, Aug 2014. doi: 10.1074/mcp.M113.036350.

[12] L Gatto, L M Breckels, S Wieczorek, T Burger, and K S Lilley. Mass-spectrometry-based spatial proteomics data analysis using pRoloc and pRolocdata. *Bioinformatics*, 30(9):1322–4, May 2014. doi: 10.1093/bioinformatics/btu013.

[13] A J Groen, G Sancho-Andrs, L M Breckels, L Gatto, F Aniento, and K S Lilley. Identification of trans-golgi network proteins in arabidopsis thaliana root tissue. *J Proteome Res*, 13(2):763–76, Feb 2014. doi: 10.1021/pr4008464.

[14] S L Hall, S Hester, J L Griffin, K S Lilley, and A P Jackson. The organelle proteome of the dt40 lymphocyte cell line. *Mol Cell Proteomics*, 8(6):1295–1305, Jun 2009. doi: 10.1074/mcp.M800394-MCP200.

[15] Jennifer Hirst, Daniel N Itzhak, Robin Antrobus, Georg H H Borner, and Margaret S Robinson. Role of the AP-5 adaptor protein complex in late endosome-to-golgi retrieval. *PLoS Biol.*, 16(1):e2004411, January 2018.

[16] D N Itzhak, S Tyanova, J Cox, and G H Borner. Global, quantitative and dynamic mapping of protein subcellular localization. *Elife*, 5, June 2016. doi: 10.7554/eLife.16950.

[17] Daniel N Itzhak, Colin Davies, Stefka Tyanova, Archana Mishra, James Williamson, Robin Antrobus, Jürgen Cox, Michael P Weekes, and Georg H H Borner. A mass Spectrometry-Based approach for mapping protein subcellular localization reveals the spatial proteome of mouse primary neurons. *Cell Rep.*, 20(11):2706–2718, September 2017.

[18] Pierre M Jean Beltran, Rommel A Mathias, and Ileana M Cristea. A portrait of the human organelle proteome in space and time during cytomegalovirus infection. *Cell Syst*, 3(4):361–373.e6, October 2016.

[19] N Nikolovski, D Rubtsov, M P Segura, G P Miles, T J Stevens, T P Dunkley, S Munro, K S Lilley, and P Dupree. Putative glycosyltransferases and other plant golgi apparatus proteins are revealed by LOPIT proteomics. *Plant Physiol*, 160(2):1037–51, Oct 2012. doi: 10.1104/pp.112.204263.

[20] N Nikolovski, P V Shliaha, L Gatto, P Dupree, and K S Lilley. Label free protein quantification for plant golgi protein localisation and abundance. *Plant Physiol*, Aug 2014. doi: 10.1104/pp.114.245589.

[21] A M Rodrguez-Pieiro, S van der Post, M E Johansson, K A Thomsson, A I Nesvizhskii, and G C Hansson. Proteomic study of the mucin gran-

ulae in an intestinal goblet cell model. *J Proteome Res*, 11(3):1879–90, Mar 2012. doi: 10.1021/pr2010988.

[22] S J Shin, J A Smith, G A Rezniczek, S Pan, R Chen, T A Brentnall, G Wiche, and K A Kelly. Unexpected gain of function for the scaffolding protein plectin due to mislocalization in pancreatic cancer. *Proc Natl Acad Sci U S A*, 110(48):19414–9, Nov 2013. doi: 10.1073/pnas.1309720110.

[23] J E Siljee, Y Wang, A A Bernard, B A Ersoy, S Zhang, A Marley, M Von Zastrow, J F Reiter, and C Vaisse. Subcellular localization of MC4R with ADCY3 at neuronal primary cilia underlies a common pathway for genetic predisposition to obesity. *Nat Genet*, Jan 2018. doi: 10.1038/s41588-017-0020-9.

[24] DJL Tan, H Dvinge, A Christoforou, P Bertone, A Martinez Arias, and KS Lilley. Mapping organelle proteins and protein complexes in drosophila melanogaster. *J Proteome Res*, 8(6):2667–2678, Jun 2009. doi: 10.1021/pr800866n.

[25] A K Tharkeshwar, K Gevaert, and W Annaert. Organellar omics-a reviving strategy to untangle the biomolecular complexity of the cell. *Proteomics*, 18(5-6):e1700113, Mar 2018. doi: 10.1002/pmic.201700113.

[26] Peter J Thul, Lovisa Akesson, Mikaela Wiking, Diana Mahdessian, Aikaterini Geladaki, Hammou Ait Blal, Tove Alm, Anna Asplund, Lars Björk, Lisa M Breckels, Anna Bäckström, Frida Danielsson, Linn Fagerberg, Jenny Fall, Laurent Gatto, Christian Gnann, Sophia Hober, Martin Hjelmare, Fredric Johansson, Sunjae Lee, Cecilia Lindskog, Jan Mulder, Claire M Mulvey, Peter Nilsson, Per Oksvold, Johan Rockberg, Rutger Schutten, Jochen M Schwenk, Asa Sivertsson, Evelina Sjöstedt, Marie Skogs, Charlotte Stadler, Devin P Sullivan, Hanna Tegel, Casper Winsnes, Cheng Zhang, Martin Zwahlen, Adil Mardinoglu, Fredrik Pontén, Kalle von Feilitzen, Kathryn S Lilley, Mathias Uhlén, and Emma Lundberg. A subcellular map of the human proteome. *Science*, 2017.

[27] M Tomizioli, C Lazar, S Brugire, T Burger, D Salvi, L Gatto, L Moyet, L M Breckels, A M Hesse, K S Lilley, D Seigneurin-Berny, G Finazzi, N Rolland, and M Ferro. Deciphering thylakoid sub-compartments using

a mass spectrometry-based approach. *Mol Cell Proteomics*, 13(8):2147–67, Aug 2014. doi: 10.1074/mcp.M114.040923.

[28] M W B Trotter, P G Sadowski, T P J Dunkley, A J Groen, and K S Lilley. Improved sub-cellular resolution via simultaneous analysis of organelle proteomics data across varied experimental conditions. *PROTEOMICS*, 10(23):4213–4219, 2010. ISSN 1615-9861. doi: 10.1002/pmic.201000359.